Experiments on laser-driven energy transfer to solid target through a foam on the ABC laser

F. Consoli[1], R. De Angelis[1], S.Yu. Gus'kov[2], A.A. Rupasov[2], P. Andreoli[1], G, Cristofari[1], G. Di Giorgio[1], D. Giulietti[3], G. Cantono[3], M. Kalal[4]

[1]*Associazione ENEA-Euratom sulla Fusione, Frascati, Italy*

[2] *Lebedev Physical Institute, Russian Academy of Sciences, Moscow, Russia*

[3]*Dipartimento di Fisica "E.Fermi" dell'Università di Pisa, Pisa, Italy*

[4]*Fac. of Nucl. Sciences and Phys. Engin., Czech Techn. Univ. in Prague, Czech Republic*

The achievement of high gains in inertial fusion confinement ICF devices is strongly determined by the stability of the imploding targets. Non-uniformities of irradiation during the early phase of laser absorption and plasma formation can act as seeds for instabilities, which would finally degrade the fuel mixing and the core plasma temperature. The use of structured materials as volume absorbers for laser radiation can be beneficial in redistributing the laser energy before it finally reaches the underlying target surface [1,2]. On the other hand, it is important that the absorber does not limit the overall energy efficiency of the process. Experiments aimed to characterize the efficiency of energy transmission through porous absorbers have been performed in the ABC laser facility in Frascati [3,4]: beam energy and intensity were about 50 J and $10^{13\text{-}14}$ W/cm^2 respectively; pulse duration was 3 ns at the basic wavelength 1054 nm of Nd-glass laser. The laser spot size was 500 μm using ISI plates as flux density profile smoothers. In this experimental campaign the absorbers were polystyrene foams of different density (10-40 mg/cm^3) and thickness (200-800 μm) in contact with metal substrates (Al, Sn). During the interaction process the laser energy is initially stored in the foam and finally released to the metal substrate by the resulting shock wave. The melting of the substrate produced by the shock wave leaves an imprint in the metal in the shape of a small crater. Measurements of the crater physical properties are shown as a function of foam thickness and interaction parameters. To characterize a foam absorber plasma interferometry, ion-collectors and soft X-ray measurements [4] have been performed as well.

Targets. Fig.1 shows three typical targets: foam on Al, pure Al, and foam on Sn. The measurements have been performed on a confocal microscope: Optical Surface Metrology System Leica DCM 3D. Resolutions higher than 45 nm on the depth, and than 1.7 μm on the plane parallel to the surface, have been used.

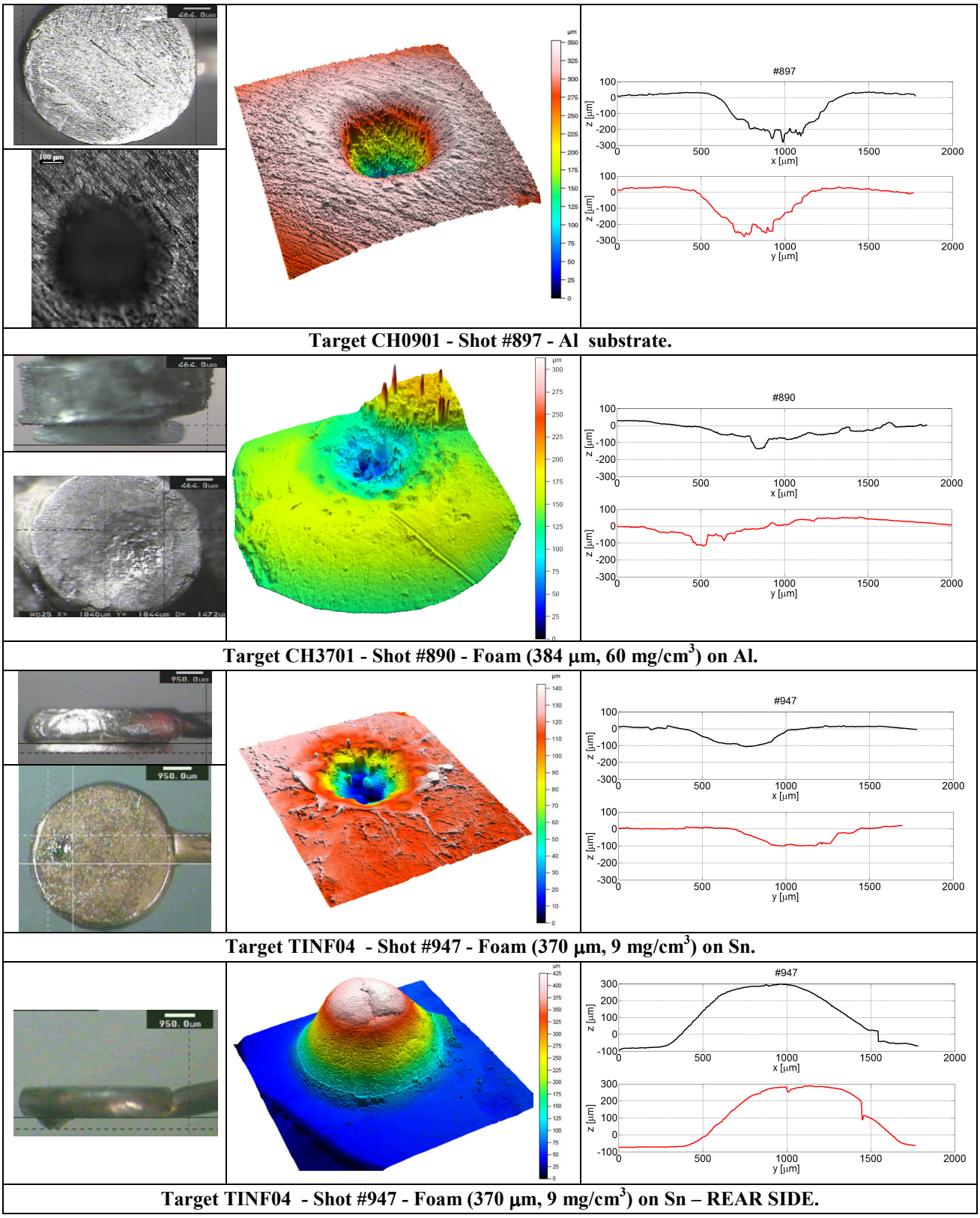

Figure 1. Data relative to the shots #890, #897, #947. Pictures before and after the shots; 2D and 3D confocal microscope measurements.

Laser-plasma characterization. The emission of particles from the plasma is monitored by ion collectors. Fig.2 shows data supplied by the Faraday cups in different shots. A peak at ion velocities = $5 \cdot 10^5$ m/s is clearly visible and corresponds to a maximum energy of

~1 keV/amu. Similar results are shown by a single crystal diamond detector (SCD464650D by Diam. Det. Ltd 'sandwich model' of 0.5 mm width). Ion discrimination by Thomson spectrometry [4] is foreseen for future shots. Apparently, shots with foam exhibit higher peak intensities than those without. Fig.3 illustrates Nomarski interferometry results for shot #890. The plasma density derived by complex interferometry [5] is also reported. X-ray continuum emission is measured by pin diodes. Temperature estimation is deduced by the ratio of the signals obtained by attenuating the incoming radiation by two Al filters (with attenuation $k(\lambda)$) of different thickness $\delta_{i,j}$ (see Fig.4). Temperatures of some hundreds of eV are estimated by comparison with the results got by the formula shown in the same Fig. 4. We are now developing a comparative temperature diagnostics using a free-standing transmission grating.

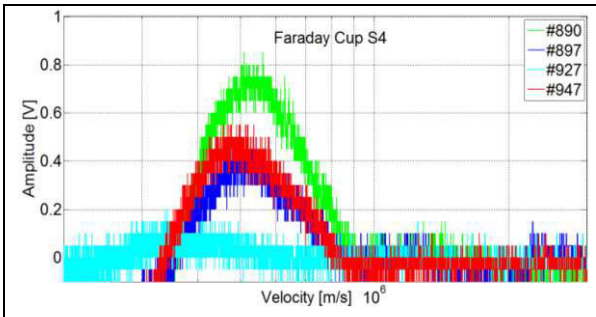

Faraday cup at θ = 42° from the laser - signal for different shots.

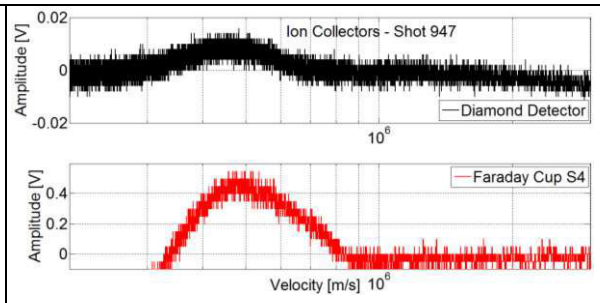

Faraday cup at θ = 42° and diamond detector at θ = 60° from the laser, for the same shot #947.

Figure 2. Information from ion collectors, for different shots. #927 is with Tin target, without foam (see Table 1).

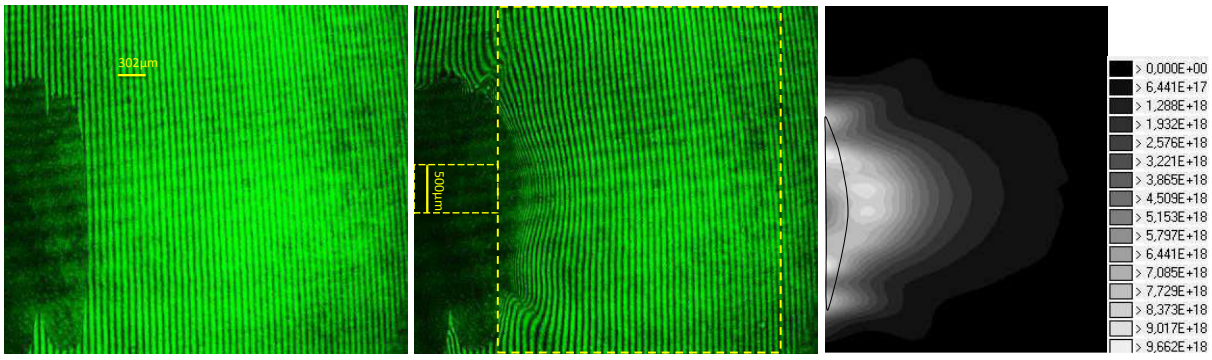

a **b** **c**

Figure 3. Shot #890 foam (384 µm, 60 mg/cm^3) on Al. Interferometry: (a) before the shot; (b) 4 ns since the shot start. Calculated profile of plasma density (electrons/cm^3) (c): region outlined by the large yellow dashed rectangle in (b). The dashed red region is the indication of the over-dense part of (b).

Discussion. In Table 1, data for different shots are given for Al and Sn substrates, with or without foam layers. Foams of different density and thickness have been used. The observed crater volumes decrease when using foam and for increasing foam densities. The effect of foam thickness appears important, and sometimes even predominant on its density. The

comparison between shots #880 and #890 shows that lower thickness may produce larger craters, even when the density is much higher. Larger craters are produced when Sn is used instead of Al (see #897, #927). In some shots with Sn substrate, a swelling was observed on the rear side of the substrate, depending on the Sn thickness. This is shown in Fig. 1 for shot #947, and the related measurements are given in Table 1. The analysis of the experiment performed, by means of theoretical modeling, is being developed.

$$\frac{E_i}{E_j}(T_e) = \frac{\int_0^{\lambda_i} \lambda^{-2} \exp\left(-\frac{12.4}{\lambda T_e} - k(\lambda)\delta_i\right) d\lambda}{\int_0^{\lambda_i} \lambda^{-2} \exp\left(-\frac{12.4}{\lambda T_e} - k(\lambda)\delta_j\right) d\lambda}$$

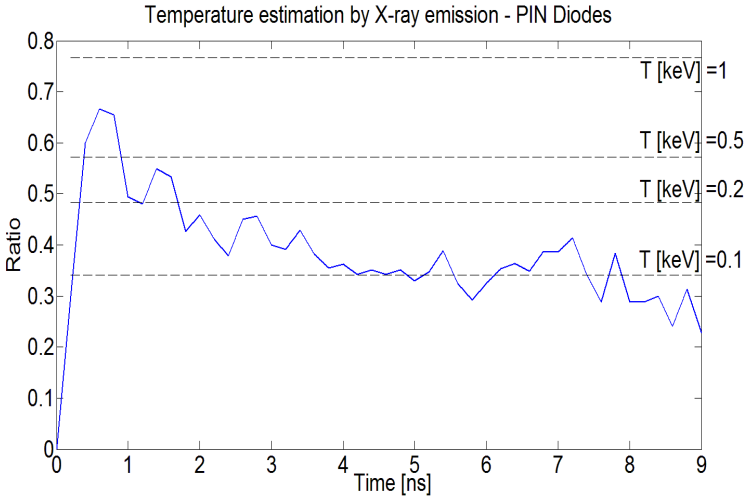

Figure 4. Shot #890 foam (384 μm, 60 mg/cm^3) on Al. Information on Temperature vs Time, achieved by PIN diode detectors.

Table 1. Data for different shots.

Shot Number	Laser Energy [J]	Target Name	Substrate material	Foam		Measured Crater		
				Density [mg/cm^3]	Thickness [μm]	Volume [mm^3]	Surface [mm^2]	Depth [μm]
897	50	CH0901	Al	NO	NO	$5.89 \cdot 10^{-2}$	0.82	332.11
911	35	CH1801	Al	NO	NO	$2.70 \cdot 10^{-2}$	1.18	209.58
880	44	CH2801	Al	10	664	$2.15 \cdot 10^{-2}$	2.02	68.06
876	42	CH1501	Al	20	788	$0.61 \cdot 10^{-2}$	1.23	30.97
899	45	CH0101	Al	40	684	$1.70 \cdot 10^{-2}$	1.72	72.87
890	49	CH3701	Al	60	384	$3.99 \cdot 10^{-2}$	1.30	161.73
927	40	TIN01	Sn	NO	NO	$8.53 \cdot 10^{-2}$	4.60	258.59
947	49	TINF04	Sn	9	370	$2.80 \cdot 10^{-2}$	1.59	122.98
						Measured Swelling		
						Volume [mm^3]	Surface [mm^2]	Height [μm]
947	49	TINF04	Sn	9	370	$23.5 \cdot 10^{-2}$	2.12	371.12

References

[1] S.Yu. Gus'kov *et al*, JETP 81, 296 (1995).

[2] S.Yu. Gus'kov *et al*, Laser Part. Beams 17, 287 (1999).

[3] A. Caruso *et al*, Laser Part. Beams 18, 25 (2000).

[4] F. Consoli *et al*, NIM A 720, 149 (2013).

[5] M. Kalal *et al,* Applied Optics 27, 1956 (1988).